Hydrodynamic Design of Underwater Gliders Using k-k$_L$-ω RANS Transition Model

Artur K. Lidtke, Stephen R. Turnock and Jon Downes
Fluid-Structure Interactions Group, University of Southampton
Southampton, SO16 7QF, United Kingdom
E-mail: A.Lidtke@soton.ac.uk, S.R.Turnock@soton.ac.uk, jon.downes@soton.ac.uk

***Abstract*—Hydrodynamic design of an underwater glider is an act of balancing the requirement for a streamlined, hydrodynamically effective shape and the consideration of the practical aspects of the intended operational envelope of the vehicle, such as its ability to deploy a wide range of sensors across the water column. Key challenges in arriving at a successful glider design are discussed and put them in the context of existing autonomous underwater vehicles (AUV) of this type. The design cycle of a new vehicle shape is then described. The discussed AUV will operate both as an buoyancy-propelled glider and a flight-style, propeller-driven submersible, utilising its large size to deliver substantial scientific payloads to remote locations to perform environmental monitoring, seabed survey, and exploration for sub-sea oil, gas and material deposits. Emphasis is put on using computational fluid dynamic (CFD) methods capable of predicting laminar-turbulent transition of the flow in order to estimate the performance of candidate designs and thus inform and guide the evolution of the vehicle. A range of considered shapes are therefore described and their hydrodynamic characteristics predicted using CFD are summarised. A final shape for the new glider is then proposed. This is then subject to an in-depth flow-field analysis which points out how natural laminar flow may be used as a means of drag reduction without compromising the practical aspects of the design, such as its ability to carry sufficient payload. Finally, the obtained data are used to project the expected glide paths, as well as give preliminary estimates of its range. These show the benefits of minimising the vehicle drag, as well as highlight the possible trade-offs between maximising speed and endurance of the AUV.**

***Index Terms*—Underwater gliders, Performance prediction, Fluid dynamics, CFD**

I. Introduction

Underwater gliders are autonomous underwater vehicles (AUV) which change their potential energy by adjusting their displacement via the use of a buoyancy engine and utilise the resulting vertical motion to generate lift, a fraction of which delivers a forward thrust force . This principle of operation is illustrated in Figure 1. The mode of propulsion employed by this category of AUVs only requires occasional actuation at the top and bottom of each tack, when extra buoyancy is being added or subtracted from the vehicle, and intermittently, primarily to compensate for changes in water density and vehicle compressibility [1], [2]. Fundamentally, this mode of locomotion relies on opposing the drag with gravity and buoyancy forces, which leads to low power consumption per unit distance travelled.

Consequently, underwater glider have seen wide use in long-endurance applications with deployments lasting of the order of months and individual vehicles travelling distances of many hundreds of nautical miles [1]. This category of vehicles is typically used in order to monitor large-scale oceanographic phenomena with length-scales of the order of 10 km and temporal scales of the order of 10 h [3]. Given the duration of their missions and nature of their service, underwater gliders are limited in terms of what sensors they may feasibly carry. Nonetheless, operators and designers, incentivised by potential savings in research ship time, are constantly looking at deploying innovative payloads increasing and the scope of application of gliders to various aspects of oceanographic research.

The aim of the present paper is to outline how modern computational fluid dynamic (CFD) methods may be used at the design stage of an underwater glider in order to better understand the effect of its hydrodynamic design, including transitional flow effects, on the expected in-service performance of the final vehicle. Specifically, a series of decisions made in the process of designing a new underwater glider are discussed and the influence of CFD on the course of the design is described. Afterwards, the most promising of the vehicle design is subjected to a more detailed fluid dynamic analysis with the aim of highlighting the key features affecting its hydrodynamic performance and their dependence on the presence of natural laminar flow. Finally, a series of predictions are made for the selected design in order to develop an understanding of the effect of the predicted flow features and overall hydrodynamic characteristics on the ability of the glider to fulfil its mission requirements.

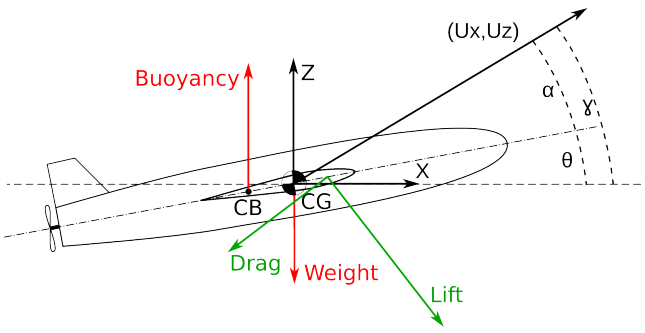

Fig. 1. Schematic representation of the principle of operation of an underwater glider. θ, α, and γ are the pitch, angle of attack, and glide path angles, respectively (forces and moments exaggerated for clearer presentation).

The presented work contributes to the EU-funded BRIDGES project (http://www.bridges-h2020.eu/). The aim of the overall project is to develop cost-effective, robust, and easily-deployed autonomous platforms capable of long-term monitoring and sensing of coastal waters and the deep ocean.

II. Underwater glider design

Underwater gliders see a wide range of very different applications, for example traversing long distances along a relatively straight path, holding station at a given location to provide persistent monitoring, or carrying out survey patterns over a geographic area or while following a certain phenomenon, such as an algal bloom [4], [5]. Another aspect to bear in mind when considering underwater glider performance is the harsh environment it operates in. This may lead to fouling appearing on the hull and lifting surfaces, causing performance to degrade over the duration of a mission at a rate which will vary with local water characteristics, such as temperature and salinity [4], [1]. Throughout its missions, the vehicle may need to sail against strong currents while trying to reach a certain geographic location, which will impede its progress and may even render it unusable for long periods of time unless it can develop sufficient forward speed. Maximising velocity could also make it easier for the vehicle to pursue scientific targets of opportunity appearing at short notice. However, increasing the maximum endurance, both in terms of range and time of deployment, may also be important for missions where the glider may follow a current, such as a west-to-east travel across the North Atlantic, or when the objective is to maintain constant location over a period of time. The design of the vehicle could be optimised to carry out a single of any of the aforementioned missions, but this would not necessarily guarantee good performance across the entire range of operations. Furthermore, versatility is a necessary trait of a glider in order to maximise the number of days it spends at sea conducting various scientific deployments, thus justifying the costs of purchasing and maintaining it. From the perspective of this work it is important to understand how these factors affect the hydrodynamic design of current vehicles and to propose a new design that will successfully carry out its duties in the future.

Forward velocities of most gliders typically do not exceed 0.5 $\mathrm{m{\cdot}s^{-1}}$. This is mainly due to the focus on promoting energy efficiency through the use of modest-sized buoyancy engines rather than at maximising their speed beyond what is necessary to sail against most currents [1], [5], [6], [7]. This translates to length-based Reynolds numbers of the order of 1 million for a 2 metre hull and less than 100,000 for hydrofoils with high aspect ratios which are typically seen on most designs [1], [3]. Therefore natural laminar flow may play an important role in determining the performance of these key glider components.

A critical consideration for an underwater glider is the glide path angle it adopts during its ascent or descent. A well understood trade-off in operating these vehicles is that minimising the glide path angles leads to increased range but also reduces the component of net buoyancy or gravity force acting against the vehicle drag and leading to a reduced speed [6], [4]. Therefore, in order to benefit from the shallow glide path angles the vehicle must maintain a high lift-to-drag ratio, L/D, since otherwise it will not be capable of propelling itself without an excessively large buoyancy engine. Since low glide angles are also generally associated with higher angles of attack [4], laminar separation on the hydrofoil sections and the hull itself is an important factor that may significantly increase the induced drag and cause a Reynolds number-dependence of the vehicle performance [8]. Another practical aspect governing the choice of glide path angles is that it is desirable to sample the data from most of the scientific sensors along the natural vertical gradients of the environmental quantities being measured [7]. Given the large scales of most oceanographic phenomena relative to the size of the vehicle, however, this may be achieved even with relatively gentle glide slopes. Most present oceanographic gliders, while capable of travelling at glide path angles as low as 10 to 15°[1], [4], typically operate at slopes around 35 to 40°[6]. This attempts to strike a balance between keeping a low induced drag and controlling the size of the buoyancy engine and the amount of energy spent on its actuation, which is typically responsible for between 60 and 80% of the energy usage on an underwater glider [6], [1], [7]. A notable exemption is the XRay blended wing glider which was designed for high transit speeds and long range with less focus for frequent vertical data profiling and hence operates at glide path slopes as shallow as 5°[2].

Since the glide slope is directly linked to the lift-to-drag (L/D) ratio [6], it may be seen as the driving force behind the chosen hydrodynamic design. Most underwater gliders develop L/D in the range of 1.5 to 5 [6], [1], while modern gliders used in air, or sail planes, on the other hand, are usually designed to have high overall L/D in excess of 20 [6]. This is because the latter are generally required to traverse large horizontal distances per unit height they lose due to gravity and are often optimised for maximum speed. An underwater glider, however, requires only a relatively small wing area per unit of hull drag in order to propel itself while minimising the proportion of the overall lift that acts against the net buoyancy force. It follows that reducing the overall system drag, and therefore the wing area, within the constraints imposed by operational requirements, is a key target for extending the range of the glider by reducing the necessary size of the buoyancy engine.

Reduction of drag may be achieved, for instance, by counteracting marine growth of the body of the glider. Another approach is to design compact glider shapes with small overall wetted surface area and to reduce the impact of sensors, protrusions and discontinuities on the overall resistance. The latter has been reported to be a crucial factor, often contributing to between 25 and 50% of the total drag [1], [9], [6], [10].

On the strictly hydrodynamic side, one may attempt to utilise the low Reynolds numbers seen of the gliders to encourage natural laminar flow (NLF), similarly to the solution adopted in the Seaglider [11], [9]. This solution poses several difficulties, for instance, designing a pressure vessel that fits into the unconventional shape and achieving surface finish and manufacturing tolerances accurate enough not to trip the flow into the turbulent regime too early. From the perspective of

a designer proposing a sound hydrodynamic shape for a new underwater glider, a better understanding of the extent of the natural laminar flow is therefore of paramount importance if an efficient vehicle is to be developed.

While the concept of applying modern numerical techniques to study the flow past autonomous underwater vehicles is not new [10], [12], [13], [14], [15], [16], [17], most of the recent work has been focused on AUVs operating at Reynolds numbers higher than those typically seen by underwater gliders. An interesting observation is also that while older work utilised methods capable of accounting for transition to turbulence at least to a certain extent [11], [18], [8], the majority of the more recent papers relied on solving Reynolds Averaged Navier-Stokes (RANS) equations using models recognised for their inability to tackle this complex physical phenomenon [19] with only a handful of exceptions [20]. A promising direction in addressing this issue is the use of more advanced flow modelling techniques, such as Large Eddy Simulation, which do not model but resolve a large proportion of turbulence. For instance, Moat *et al.* [21] discuss how such methods may be used to understand the effect of local geometric features on an underwater glider. Numerical approaches from this category are, however, prohibitively expensive and hence cannot be reliably used at the design stage. The present work therefore investigates the uses of the $k_L - k_T - \omega$ RANS model by Walters and Cokkjat [22] in order to account for the presence of transition in the flow and provide more realistic performance estimates for the new underwater glider design.

III. Methodology

A. Turbulence modelling

All of the performed fluid dynamic simulations are carried out using steady, incompressible Reynolds averaged Navier-Stokes (RANS),

$$\nabla \cdot \overline{\mathbf{U}} = 0, \tag{1a}$$

$$\left(\overline{\mathbf{U}} \cdot \nabla\right) \overline{\mathbf{U}} + \nabla \cdot \left(\overline{\mathbf{u}'\mathbf{u}'}\right) = -\frac{1}{\rho}\nabla \overline{p} + \nu \nabla^2 \overline{\mathbf{U}} \tag{1b}$$

In the above $\mathbf{U}$ is the fluid velocity, p is the pressure, ρ is the density, and ν is the kinematic viscosity. The overline notation indicates an ensemble average and $\rho\nabla \cdot \left(\overline{\mathbf{u}'\mathbf{u}'}\right)$ is termed the Reynolds' stress tensor and represents the action of turbulence on the mean flow. Due to its non-linearity the latter term is modelled rather than solved for in order reduce the computational effort. The governing equations are solved using an implicit SIMPLE algorithm implemented in the OpenFOAM framework [23], a set of open-source libraries and utilities aimed at numerical solution of partial differential equations. The approach relies on discretising the equations using the finite volume method and solves them in an iterative manner.

To provide benchmark results, the Reynolds stress tensor is first modelled using the Menter $k - \omega\, SST$ model [24], arguably the most common choice in simulating flow past underwater vehicles [16], [15], [14], as well as ship hulls [25], [26]. It uses two additional variables, the turbulent kinetic energy, k, and the specific dissipation rate, ω, to provide expressions for the turbulent length and time scales. These are then used to yield a scalar variable, the turbulent viscosity ν_T. This quantity aims to relate the rate of strain in the mean flow to the action of turbulence to the mean flow following the Boussinesq hypothesis. Exact details of the model are discussed by Menter [24]. This model does not account for the occurrence of transition well, effectively predicting fully turbulent flow over most of the tested geometries. From the perspective of underwater glider design, the results obtained using this approach may be viewed as a scenario in which local discontinuities, such as scratches, dirt, joints, etc., cause the flow to transition almost immediately.

In order to predict transition to turbulence the $k_T - k_L - \omega$ model by Walters and Cokkjat [22] is also used in the present work. This model solves three transport equations for turbulent kinetic energy, k_T, specific dissipation rate, ω, and laminar kinetic energy, k_L. The latter is used to determine where laminar instabilities render the flow turbulent and hence onset of transition may be captured. Fundamentally, this builds on similar principles to the Menter model although an additional transport equation for the laminar kinetic energy is solved, yielding

$$\begin{aligned}\frac{\mathrm{D}k_T}{\mathrm{D}t} &= P_{k_T} + R_{BP} + R_{NAT} - \omega k_T - D_T \\ &\quad + \frac{\partial}{\partial x_j}\left[\left(\nu + \frac{\alpha_T}{\sigma_K}\right)\frac{\partial k_T}{\partial x_j}\right],\end{aligned} \tag{2a}$$

$$\frac{\mathrm{D}k_L}{\mathrm{D}t} = P_{k_L} - R_{BP} - R_{NAT} - D_L + \frac{\partial}{\partial x_j}\left[\nu \frac{\partial k_L}{\partial x_j}\right], \tag{2b}$$

$$\begin{aligned}\frac{\mathrm{D}\omega}{\mathrm{D}t} &= C_{\omega 1}\frac{\omega}{k_T}P_{k_T} - C_{\omega 2}\omega^2 + C_{\omega 3} f_\omega \alpha_T f_w^2 \frac{\sqrt{k_T}}{d^3} \\ &\quad + \left(\frac{C_{\omega R}}{f_W} - 1\right)\frac{\omega}{k_T}\left(R_{BP} + R_{NAT}\right) \\ &\quad + \frac{\partial}{\partial x_j}\left[\left(\nu + \frac{\alpha_T}{\sigma_w}\right)\frac{\partial \omega}{\partial x_j}\right],\end{aligned} \tag{2c}$$

where the terms on the right-hand-sides of the equations denote production, destruction and transport of the basic turbulent quantities. This is discussed in detail in the work of Walters and Cokkjat [22].

The key concepts of the present transition model are that the total kinetic energy of fluctuations in the flow, $k_T + k_L$, is assumed to be produced proportionally to the mean strain rate in the fluid. Linear coefficient, $P_{k_L} = \nu_{T,1} S^2$, is also assumed to govern this relationship.

B. Mesh generation

Unappended glider hull simulations are performed using structured hexahedral grids. Due to more complex geometry, the proposed glider shape including foils, tail fin, and stabilisers, has been meshed using unstructured tetrahedra meshes with prism boundary layer cells. An example of such a grid is presented in Figure 2. The outer domain shape (seen in Figure 2a) is a hemisphere with radius equal to 10 vehicle lengths. Approximately 3 million cells are used to resolve the flow around half of the vehicle in the scenarios where fully-appended designs are being considered. All meshes are

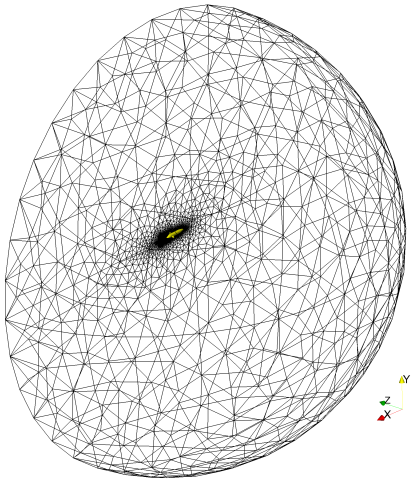

(a) Domain

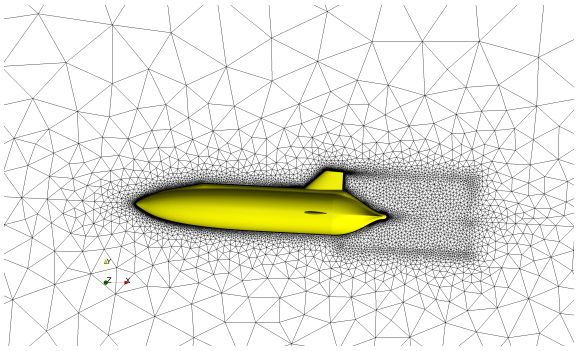

(b) Free-stream near the hull

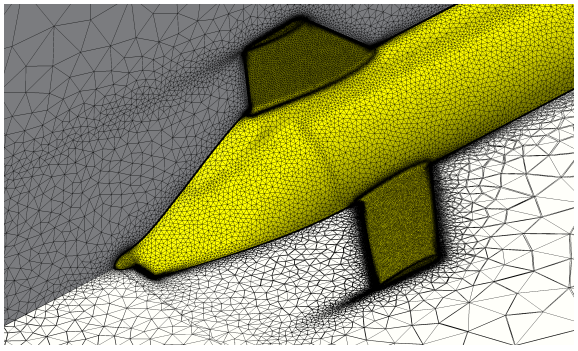

(c) Stern area

Fig. 2. View of the unstructured, tetrahedral mesh used to compute the flow around the underwater glider.

generated using Pointwise [27] and are designed with the non-dimensional wall-normal mesh size of $y^+ \leq 1$ in order to resolve the inner regions of the boundary layers.

C. Simulation set up

In the governing flow equations, the convective terms are discretised using second-order upwind scheme and turbulent quantities are treated with first-order upwind stencils. Steady flow is assumed and hence the time derivatives are dropped. Coupling between the pressure and velocity is solved using an implicit, segregated SIMPLE algorithm. The systems of equations are solved until convergence of L_1 norm to at least 10^{-6} has been achieved. The fully-appended hull simulations required approximately 48 hours to evaluate a single operational point (speed and angle of attack) on 32 processors.

In all of the simulations inlet turbulence levels of 0.2% are used with eddy viscosity ratios of approximately 100. These correspond to typical high-quality wind tunnel conditions, although the values encountered by the glider in service may vary depending on the environment it operates in and future sensitivity studies will need to be carried out to better understand the effect of these quantities on achieved performance. For each case a symmetry plane condition is used to allow only half of the design to be simulated, thus reducing the cell count substantially. A no-slip boundary condition is applied on the glider and all its appendages while free-stream inlet-outlet conditions is applied to the hemispherical outer domain. The latter adjusts automatically between an inlet and an outlet depending on the orientation of the free-stream velocity vector to the face normal vector, thus allowing for the flow to freely exit the domain downstream of the vehicle.

The present model has been validated based on a number of test cases: flat plate with and without axial pressure gradients (T3 [28]), natural laminar flow body [29], low-Re SD7003 foil [30], and a symmetric SD8020 foil section [31]. Details of the process are described in [32]. Overall, the validation study has indicated that the current numerical set up models the principle physics involved in natural transition well across a range of flow regimes representative of what underwater gliders may experience in service. Most importantly, it has been able to predict the force coefficients acting on streamlined shapes and accounts for the effect of stream-wise pressure gradient. These two features are of key importance to being able to use the model to select more hydrodynamically sound designs.

IV. Design process of a new glider

A. Specification

At the outset of the presented work the only available information about the vehicle were its maximum size, approximate mass and buoyancy engine capacity, as well as an estimated volume necessary to accommodate the pressure vessel and wet subsystems. The primary requirement of the glider was that it should be able to achieve the minimum forward speed of 0.25 $\mathrm{m{\cdot}s^{-1}}$ at less actuation than the maximum capacity of the engine and that it should allow for typical oceanographic measurements across the water column to be carried out. A unique feature of the vehicle is that it is intended to carry a dual propulsion system, traversing long distances as a glider and performing localised surveys as a classical, propeller-driven AUV when on station. This signifies not only the importance of achieving satisfactory glide performance, but also the necessity to minimise drag at the level-keep condition, as well as maintaining a satisfactory propeller inflow profile.

The design process of the glider hydrodynamic shape was divided into three stages,

1) Design of the axisymmetric hull,
2) Addition of the hydrofoils, stabilisers and the rudder,
3) Incorporation of other fairings.

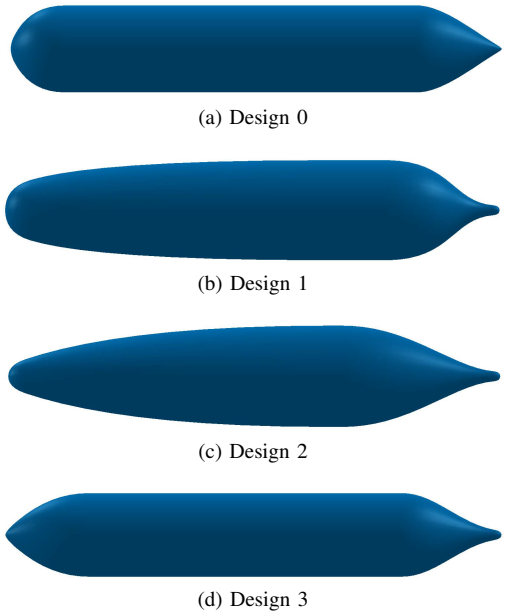

(a) Design 0

(b) Design 1

(c) Design 2

(d) Design 3

Fig. 3. Concepts of initial axi-symmetric hull designs (flow from left to right). Designs scaled to the same unit-length.

This allowed the design space to be progressively narrowed down, therefore limiting the number of possible design paths and necessary fluid dynamic simulations to be carried out. At each of these stages a series of possible designs was created. Hydrodynamic characteristics of each of them were then simulated and the results compared in order to guide the decision-making process.

B. Hull form shape selection

Figure 3 presents candidate designs used to evaluate the effect of the underlying axi-symmetric part of the glider hull on the overall system performance. Design 0 is a Myring body [33] with parallel sides and a conical stern, similar to several commercially available AUVs and underwater gliders. Designs 1 and 2 provide an identical enclosed volume but have the maximum cross-section area point shifted aft in order to induce a favourable pressure gradient over a large proportion of the hull, thus encouraging natural laminar flow [29]. Design 3 is a more streamlined Myring shape. Each of the hulls was designed to house a pressure vessel of given size, to meet length and width constraints and to provide enough useful volume for sensors and other pressure-resistant subsystems.

Flow past each of the designs was computed over a range of Reynolds numbers corresponding to nominal and maximum speeds expected on the glider and an angle of attack of 3 degrees. The latter was chosen as the target value for the glider in order to maximise performance of the hydrofoils based on 2D section characteristics.

Table I presents the lift and drag coefficients of the considered designs computed using the turbulence model capable of predicting transition. These are defined as

$$C_L = \frac{L}{\frac{1}{2}\rho U^2 (\Delta/\rho)^{\frac{2}{3}}}, \tag{3a}$$

TABLE I

FORCE COEFFICIENTS DEFINED USING $(\Delta/\rho)^{\frac{2}{3}}$ FOR THE PRELIMINARY HULL SHAPE DESIGNS COMPUTED ASSUMING FREE TRANSITION. CALCULATIONS AT TWO FIXED OPERATING POINTS WITH AN ANGLE OF ATTACK OF 3° AND TWO DIFFERENT REYNOLDS NUMBERS DEFINED USING THE TOTAL LENGTH OF THE HULL. C_{Di} IS THE INDUCED DRAG COEFFICIENT, COMPUTED AS THE DIFFERENCE BTWEEN THE TOTAL DRAG COEFFICIENT AND THE VALUE AT ZERO INCIDENCE ANGLE TO THE FLOW.

Design	C_D	C_{Di}	C_L	L/D
Re_L 1.5 million				
0	4.49E-3	9.37E-5	4.40E-4	0.10
1	4.83E-3	1.86E-4	6.81E-4	0.14
2	2.14E-3	1.20E-4	1.26E-3	0.59
3	3.14E-3	4.46E-3	7.62E-4	0.10
Re_L 3.0 million				
0	4.22E-3	3.97E-5	8.43E-4	0.20
1	2.23E-3	-1.28E-3	4.30E-4	-0.48
2	1.51E-3	1.36E-4	7.49E-4	0.50
3	4.02E-3	2.94E-3	2.83E-4	0.04

$$C_D = \frac{D}{\frac{1}{2}\rho U^2 (\Delta/\rho)^{\frac{2}{3}}}, \tag{3b}$$

using the dry mass, Δ, and the displaced fluid volume, Δ/ρ, in order to define a reference area for non-dimensionalisation. This convention has been chosen in order because it is deemed to better reflect the drag that needs to be overcome to transport a unit volume of subsystems than a notation based on wetted surface area. It can be seen that design 2 has been predicted to produce both more lift and have a lower drag than the other designs, despite a relatively high surface area. This may be attributed to the boundary layer remaining laminar over a large proportion of the hull compared to the other designs, which limits the friction drag constituting approximately 70% of the total resistance. This is caused by the stream-wise pressure gradient remaining favourable up to the maximum cross-section area. One way to envisage this is to observe that a particle carried by the flow close to the hull surface would experience reducing pressure since the moment it moved past the bow and travelled up to the point of maximum hull radius. At the nominal Reynolds number, other designs offer comparable performance in terms of lift-to-drag ratio. At the higher speed, design 1 suffers from significant flow separation on the suction surface leading to a negative lift coefficient. In this condition design 3 experiences slightly less drag than design 0 but produces up to five times less lift.

Figure 4 presents an example result of the stream-wise velocity contours predicted using the transition model for designs 0 and 2. It is worth noting how the natural laminar flow design only has one inflection point, which leads to a steady, favourable pressure gradient over most of the hull while the Myring shape induces regions of high velocity, and thus low pressure, at both ends of the parallel mid-body. This causes the flow to transition much sooner than for the former design, leading to a thick, turbulent boundary layer and a wide wake. Both of these effects lead to approximately 50% increase in drag compared to design 2.

It is also vital to understand how important the natural

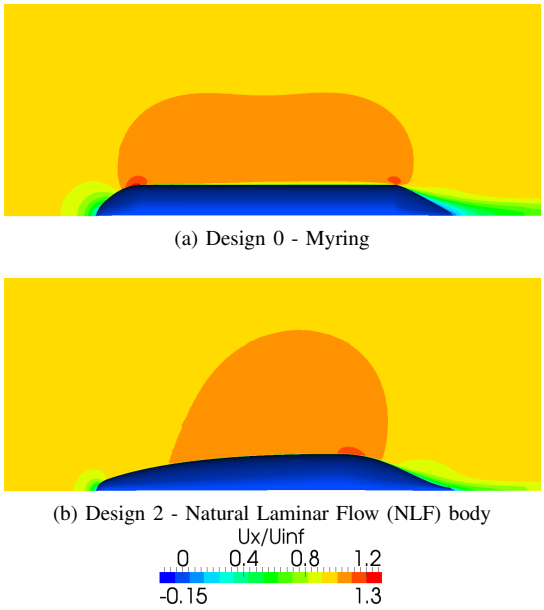

(a) Design 0 - Myring

(b) Design 2 - Natural Laminar Flow (NLF) body

Fig. 4. Stream-wise velocity contours for two different AUV hull shapes. Flow from left to right, local curvature causing flow acceleration implies change of the pressure gradient likely to encourage transition to turbulence.

TABLE II
FORCE COEFFICIENTS FOR THE CHOSEN PRELIMINARY HULL SHAPE DESIGNS ASSUMING FULLY TURBULENT FLOW (DEFINED USING $(\Delta/\rho)^{\frac{2}{3}}$) AT AN ANGLE OF ATTACK OF 3°.

Design	C_D	C_{Di}	C_L	L/D
Re_L 1.5 million				
0	8.31E-3	2.58E-4	-2.06E-4	-0.02
2	7.20E-3	1.03E-4	1.79E-3	0.24
0	7.26E-3	3.22E-4	-7.75E-4	-0.10
2	6.29E-3	6.39E-3	1.70E-3	0.27

transition is in governing the performance of the hull. In a real environment the vehicle will be subject to various free-stream turbulence levels, surface roughness and assembly imperfections, all of which may trip the flow to become turbulent earlier than the idealised CFD result would suggest. Table II presents the force coefficients for designs 0 and 2 computed using the $k-\omega\,SST$ model, which leads to the transition occurring almost immediately. Overall, both designs may be seen to exhibit much higher drag in the fully turbulent scenario than when transition to turbulence is considered. However, in the present case the Myring design produces 15% less drag than the NLF hull when subject to an angle of incidence of 3°. This is mainly due to the lower wetted surface area for the same useful enclosed volume of the former concept. It is therefore crucial for the designer to make sure that laminar flow will indeed be present in reality if the NLF hull form is to be selected, because otherwise this design will ehibit worse performance than the parallel-sided solution.

C. Appended hull characteristics

Based on the preliminary design concept exploration, three candidate shapes for the final design were considered. These were based on the NLF hull concept (design 2), given it has been found to offer favourable characteristics in the more realistic natural transition scenario and performed nearly as well as its competitors in the pessimistic fully turbulent case. A vertical stabiliser fin was also added, together with horizontal stabilisers, intended to shift the centre of lift aft and thus render a more neutral pitch balance. This was needed because of the centre of gravity of the vehicle being placed unfavourably due to the internal arrangement.

A parallel study was carried out in order to investigate appropriate section shapes and planforms for the hydrofoils. This relied heavily on the public low-Reynolds number airfoil experimental database by Selig *et al.* [31]. Figure 5 presents the lift curves of the short-listed airfoil shapes. Based on an assumed lift distribution, bare hull drag predicitons, preliminary buoyancy engine capacity estimates, and suitable margins accounting for added drag due to fairings and discontinuities, a preliminary planform of the foil could be devised. This was later studied numerically in isolation, with key observations summaries by [34]. Following this, a hydrofoil shape based on the J5012 shape was fitted to the vehicle model. It was designed to have a possibly high aspect ratio in order to increase the overall hydrodynamic efficiency. The target L/D ratio of the overall vehicle was aimed to be approximately 5, which should provide sufficient capability in executing the intended portfolio of missions. Minimum chord was kept above 200 mm, which is a typical value representative of foils used on present gliders, and should limit the possibility of stall at slow speeds [3] while keeping the wing span within the vehicle footprint constraints.

Finally, additional fairings accommodating sensor payloads and structural elements were also integrated into the upper part of the hull. A segment of parallel mid-body also had to be accommodated in order to allow easier integration of the cylindrical pressure vessel. This resulted in designs 4, 5, and 6 being created, shown in Figure 6. The major differences between them were the shape of the after body affecting the wake and laminar separation. Lift and drag characteristics for

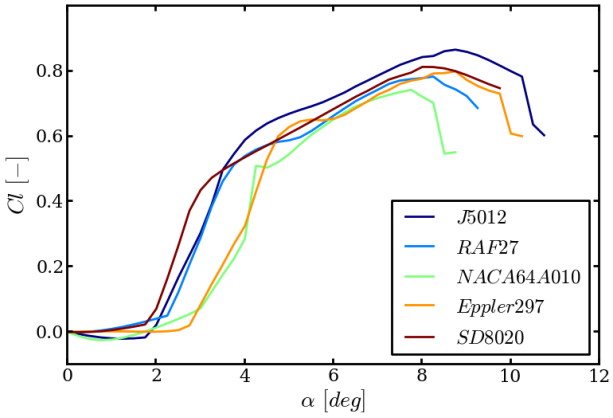

Fig. 5. Lift coefficient data for the airfoil shapes considered as candidates to be fitted to the present vehicle. Data from [31].

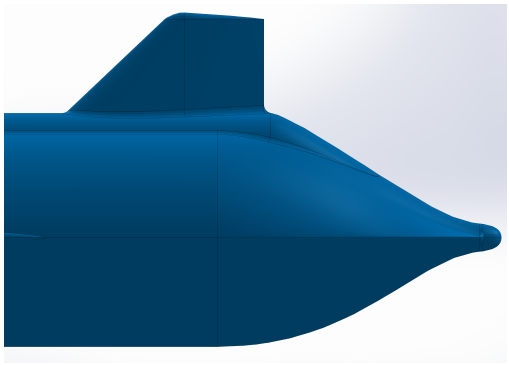

(a) Design 4

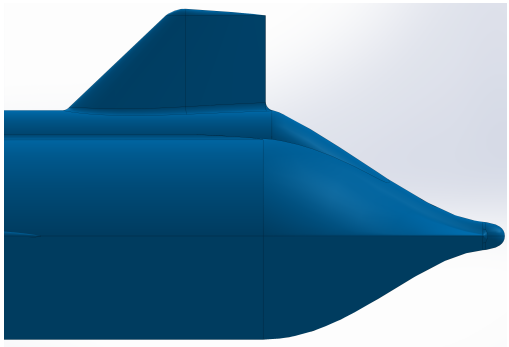

(b) Design 5

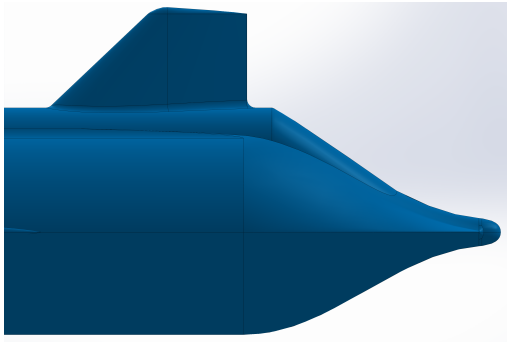

(c) Design 6

Fig. 6. Different stern shapes considered in the detailed design study.

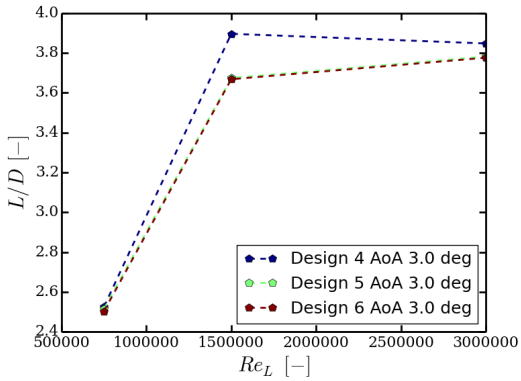

(a) Free transition

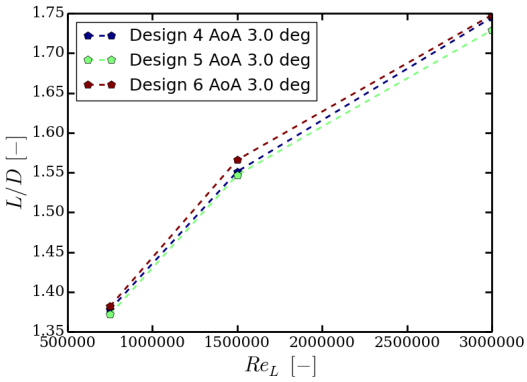

(b) Turbulent

Fig. 7. Lift to drag ratios predicted for the three intermediate designs.

each design were then computed using CFD across a range of expected speeds and at the target angle of attack of 3°. Length-based Reynolds number corresponding to the target maximum speed is approximately 1.5 million and 750,000 for the nominal velocity the glider is expected to encouter during most of its service.

Figure 7 presents the predicted lift-to-drag ratios for all of the developed designs. The scenario where transition is allowed to occur naturally allowed each of the vehicles to achieve much lower drag than in the fully turbulent evaluation, leading to significantly higher L/D. Furthermore, due to its stern shape allowing a more gentle pressure recovery design 4 has outperformed the other design candidates in terms of the L/D parameter by approximately 5% over the lower range of Reynolds numbers corresponding to typical gliding conditions. In the fully turbulent case the differences between all of the shapes were minimal as their wetted surface areas were very comparable. It should be noted that most of the lift was generated by the hydrofoils and hence most of the observed differences are due to a difference in drag induced by the hulls. The presented L/D estimates also indicate that even in the most pessimistic scenario the new glider should be able to at least match existing designs in terms of achieving the preferred glide path range between 30 and 40°.

D. Selected design performance prediction

Based on the results presented in the previous section, a candidate shape of the glider has been proposed, as shown in Figure 8. It is virtually identical to the best-performing design 4 except the longitudinal positions of the hydrofoils have been adjusted from the baseline configuration to provide more a favourable pitch balance. This entailed shifting the foils further aft of the longitudinal position of the centre of gravity in order to provide a larger restoring moment when a pitch angle is applied. This will act to compliment the restoring pitch moment generated by the tapered shape of the stern forming horizontal stabiliser surfaces. In service this is expected reduce the amount of actuation of the movable mass system needed to maintain a stable glide in the vertical plane.

Figure 9 shows the change of non-dimensional drag on the chosen glider shape as a function of Reynolds number and angle of attack. It is apparent that if the flow is assumed to be fully turbulent the resistance increases, primarily due to the

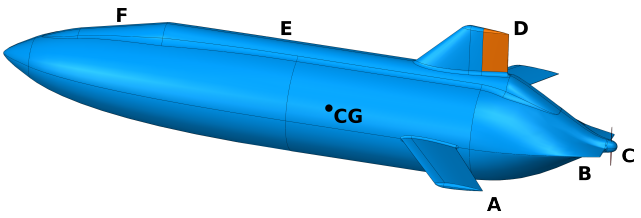

Fig. 8. Final underwater glider design evaluated; A - hydrofoil, B - horizontal stabiliser, C - propeller, D - tail fin (movable part highlighted in orange), E - central fairing for structural frame, F - fairing for a CTD sensor, CG - centre of gravity.

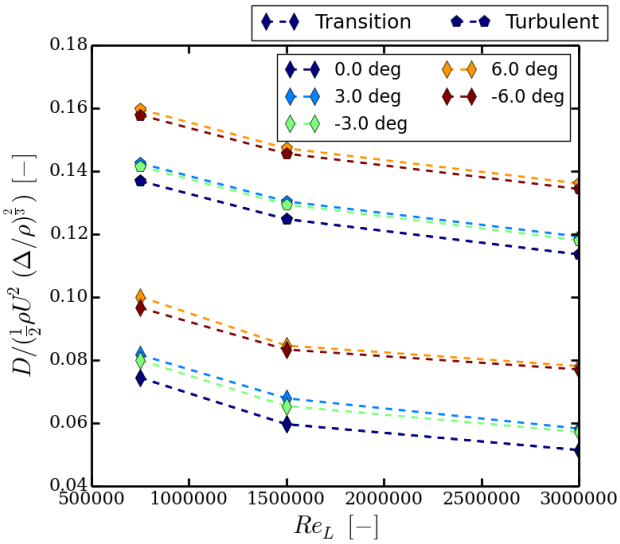

Fig. 9. Drag area estimate for the final design as a function of Reynolds number assuming both natural transition and fully turbulent flow. The influence of induced drag at the design angle of attack of 3°and higher 6°also indicated.

nearly thee-fold increase of the friction drag. At the same time, assuming natural transition leads to an increase of pressure drag by 8% compared to the fully turbulent scenario, but this penalty is small compared to the viscous drag coefficient change.

Rudnick *et al.* [1] reported that the current Slocum and Spray gliders are characterised by approximately constant drag area over a range of operational Reynolds numbers, while the Seaglider exhibits a reduction in the drag area as the Reynolds number increases which is caused by its natural laminar flow hull. In the present datasets a slight reduction in drag coefficient is seen as a function of Reynolds number, although the predicted curve has a lower slope than was reported for the Seaglider and appears to reach a plateau as the vehicle nears its maximum speed. It is also worth noting that the induced drag coefficient varies slightly for the present hull depending on whether positive or negative angles of attack are adopted. This is due to the top-bottom asymmetry of the AUV associated with the presence of the central sensor fairing and the vertical fin on the upper side of the hull.

In the selected design, the pitch stability has been regarded as a crucial hydrodynamic characteristic and substantial care was put into placing the hydrofoils at a favourable longitudinal

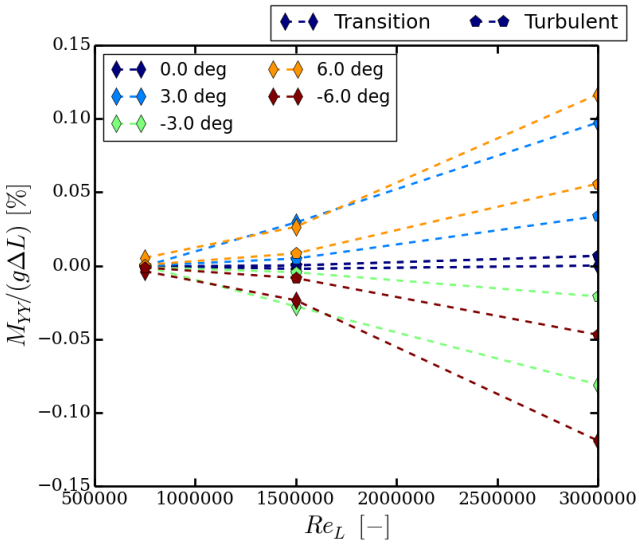

Fig. 10. Pitch moment coefficient about the centre of gravity acting on the final design shown as a function of Reynolds number and angle of attack.

position. The target result was to achieve neutral pitch balance at the nominal velocity so that the pitch actuation control can rely primarily on adjusting the hydrostatic balance. At higher speeds the glider system delivers a restoring moment which should help in pointing it into the flow and thus reducing the actuation required of the movable mass system. This data is shown in Figure 10. Non-dimensionalisation was chosen to reflect the magnitude of the moment generated at each speed relative to the size of the movable mass system.

V. Understanding the Flow Past the Glider

The flow field around the glider has been analysed in more detail in order to develop a deeper understanding of what makes it perform better than the considered alternatives and to suggest possible future improvements. Figures 12 and 11 compare pressure and skin-friction coefficient distributions for the final design computed using both the transition model and the ”fully turbulent” approach. These were calculated for the maximum target glide speed and the nominal angle of attack of 3°. One can note that the pressure distributions are very comparable in both cases, with only noticeable differences occurring around the stern in the pressure recovery region. The skin friction coefficient has been predicted to have an overall similar distribution but the SST model predicted higher viscous forces over most of the hull, yielding a higher integral value. This further corroborates the observations made based on total force coefficients. Moreover, the pressure coefficient plots show how the shape of the forebody induces a favourable pressure gradient over a large portion of the hull, which should have a beneficial effect on forestalling transition to turbulence. However, the present shape of the CTD sensor fairing at the bow may be seen to cause a local acceleration to the flow, thereby having an adverse effect on the adopted drag minimisation strategy. This will therefore need to be addressed in the future iterations of the design before the first prototype is built.

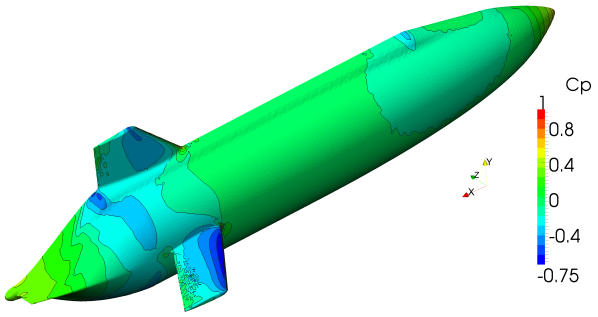

(a) Natural transition - $k_L - k_T - \omega$

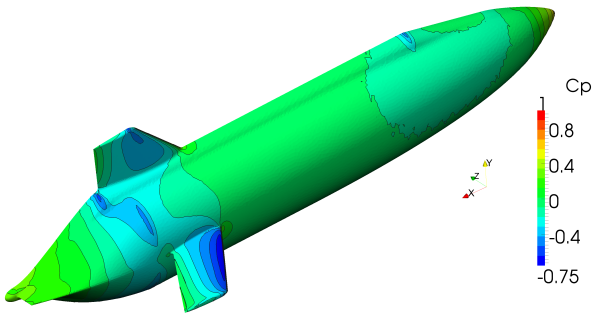

(b) $k - \omega\, SST$

Fig. 11. Pressure coefficient distribution on the final design at an angle of attack of 3°and Re_L 1.5 million predicted using two turbulence models.

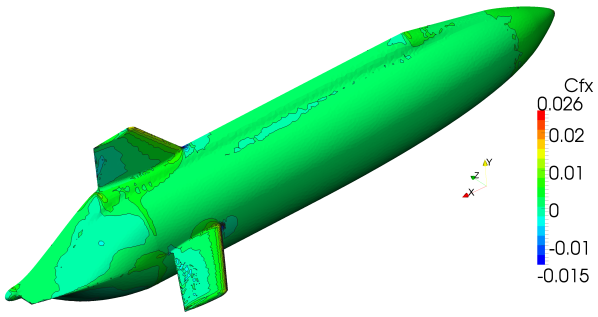

(a) Natural transition - $k_L - k_T - \omega$

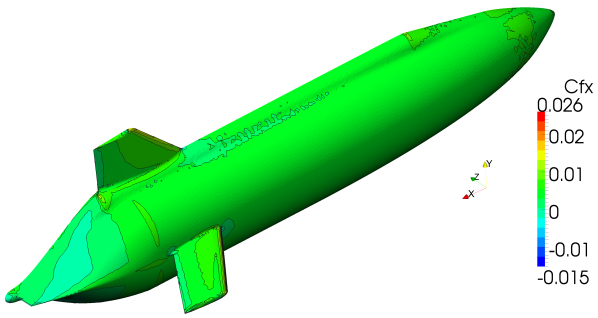

(b) $k - \omega\, SST$

Fig. 12. Skin-friction coefficient distribution on the final design at an angle of attack of 3°and Re_L 1.5 million predicted using two turbulence models.

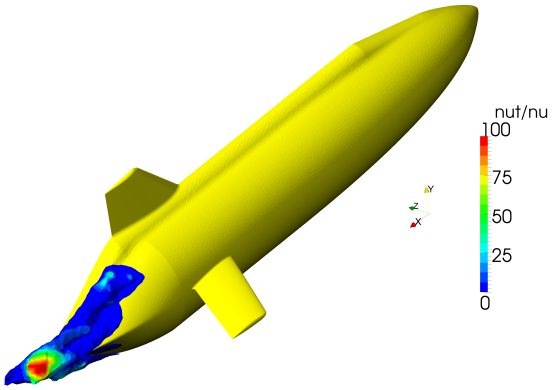

(a) Natural transition - $k_L - k_T - \omega$

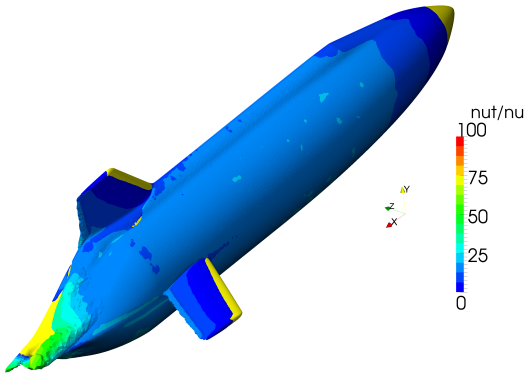

(b) $k - \omega\, SST$

Fig. 13. Iso-contour of turbulence intensity of 5% coloured by non-dimensional eddy viscosity predicted for the final design at an angle of attack of 3°and Re_L 1.5 million using two turbulence models.

Figure 13 presents iso-contours of turbulence intensity around the hull at the maximum glide speed and nominal angle of attack coloured by eddy viscosity. The latter highlights the regions in which the RANS model is particularly active and affects the overall flow solution. If free transition is considered, high turbulence intensity is not encountered until the fluid reaches the parallel mid-body and transitions due to the lack of a favourable pressure gradient. When the SST model is used, however, turbulent kinetic energy (TKE) production in the boundary layer contributes to high TKE levels from relatively early on in terms of local Reynolds number.

Figure 14 depicts streamlines computed for fluid particles close to the centreline of the AUV at the maximum glide speed and nominal angle of attack of 3°. These are coloured by the local pressure coefficient. One can note how the flow at the underside of the AUV sees continuous favourable pressure gradient up to the stern which is expected to have a beneficial effect on encouraging natural laminar flow. On the upper side of the vehicle adverse pressure gradient starts to occur approximately at amidships. An important observation is the inception of a vortex at the radius between the central fairing and the hull surface which starts to take place around the leading edge of the vertical fin.

Figures 13 and 14 have indicated the presence of a top-bottom asymmetry in the flow, particularly if the fully turbulent scenario is considered. Figure 15 examines the axial flow and turbulence intensity at x/L 99% from the bow with the

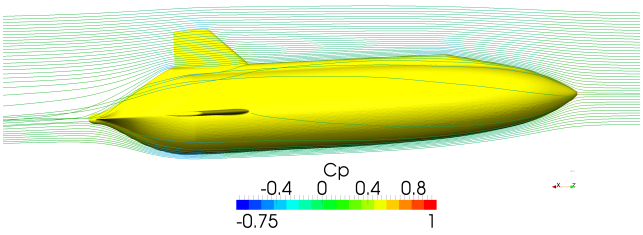

Fig. 14. Streamlines computed for the final design at an angle of attack of 3°and Re_L 1.5 million using the transition model.

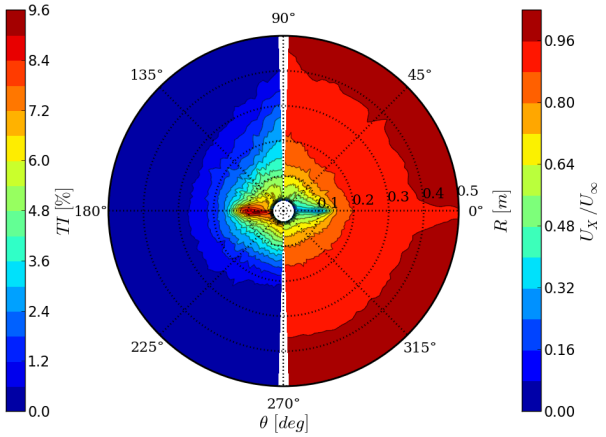

(a) Natural transition - $k_L - k_T - \omega$

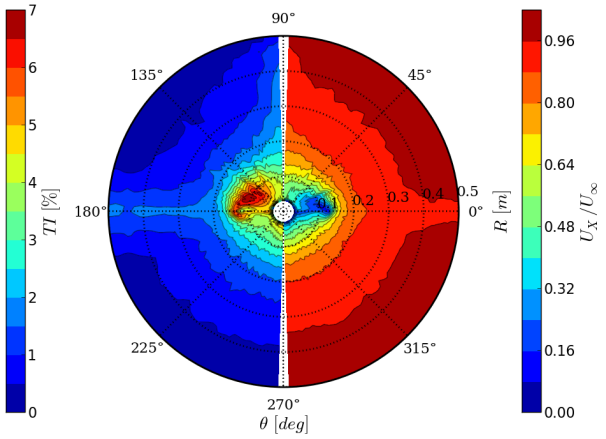

(b) $k - \omega\, SST$

Fig. 15. Iso-contours of the turbulence intensity (left) and axial velocity (right) behind the stern of the vehicle at x/L 0.99 predicted using the two RANS models.

vehicle at a nominal forward speed and level keel in order to further explore the origins of this observation. One may note how in the fully turbulent scenario a much stronger vortex is predicted to be generated by the flow over the rudder and top fairing, which manifests itself as a strong wake non-uniformity. While the effect of this flow feature has been shown to have a minimal effect on the force coefficients, it will have a prominent impact on the design of the propeller for the vehicle, which shall be addressed at the future design stages.

VI. Predicting Service Performance

As previously discussed in this paper, underwater gliders must be able to balance speed and endurance requirements depending on the type of mission they are undertaking. In order to characterise the performance of the present vehicle, it is useful to therefore consider two scenarios - one which maximises horizontal speed without consideration for the glide path angle and endurance, and one which attempts to maintain a low glide path angle and thus increase the vehicle range.

This first step in evaluating the performance envelope of the designed vehicle was to assume a range of pitch angles that a glider could adopt thanks to its ability to shift the centre of gravity position longitudinally and find a point at which the forces acting on the system are in equilibrium,

$$\sum_i F_{x,i} = 0, \tag{4a}$$

$$\sum_i F_{z,i} = 0. \tag{4b}$$

This involved solving a problem with two free variables, horizontal and vertical speed, the ratio of which affects the real glide path angle, which is different to the assumed pitch inclination (see Figure 1).

Figure 16 presents this data for the proposed final glider shape subject to three different vertical forces corresponding to minimum, nominal, and maximum intended actuation of the buoyancy engine. The lift and drag coefficients were computed using CFD as a function of the angle of attack and Reynolds number using the transition and fully turbulent RANS models. The simplified equations of motion were then solved numerically using the regressed CFD data until balance of forces for each pitch angle has been found.

Notably, that the predictions made using the transition model yield a much more optimistic estimate of forward speeds of the glider, mainly due to the reduced drag. Moreover, the data suggests shallower glide path angles may be obtained in the natural transition scenario with near-optimum forward velocities being reached at angles about of 30°, compared to 40° for the fully turbulent results.

It has also been confirmed that the design should be able to achieve the desired maximum speed with buoyancy engine capacity within the range used by the presently used underwater gliders (these have reported ballast fractions of Slocum - 0.87%, Spray - 1.76% and Seaglider - 1.62% of total vehicle mass [1]). The present estimates do not include the added drag due to sensors which, as already pointed out, may be significant. Present estimates indicate, however, that sufficient margin exists in the design to still allow the speed requirements to be met even if the drag increases substantially.

Using the speed envelope, it was possible to compute the expected trajectory of the glider. Figure 17 shows the paths predicted for the vehicle in both the fully turbulent and free-to-transition flow models obtained using the medium buoyancy engine setting and an assumed typical motion amplitude of 1000 m [35]. The data was obtained for two scenarios - one assumed the vehicle moving at the maximum forward speed at a steep glide path angle, and the other followed a

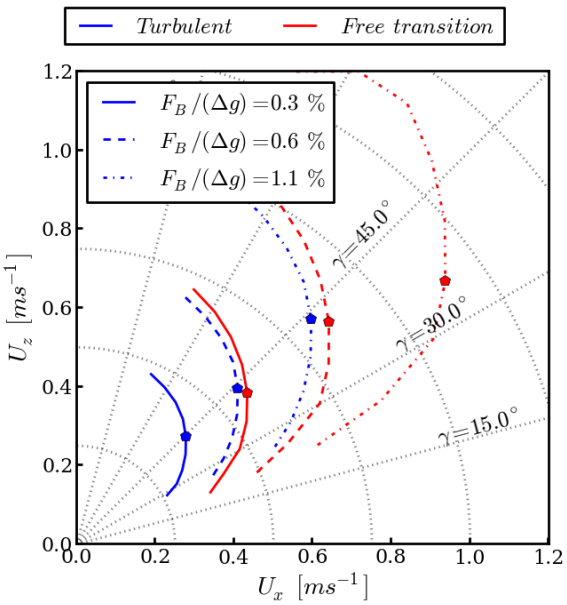

Fig. 16. Performance envelopes for the proposed underwater glider design as computed using data from two different turbulence models. F_B denotes a constant vertical force induced by a buoyancy change.

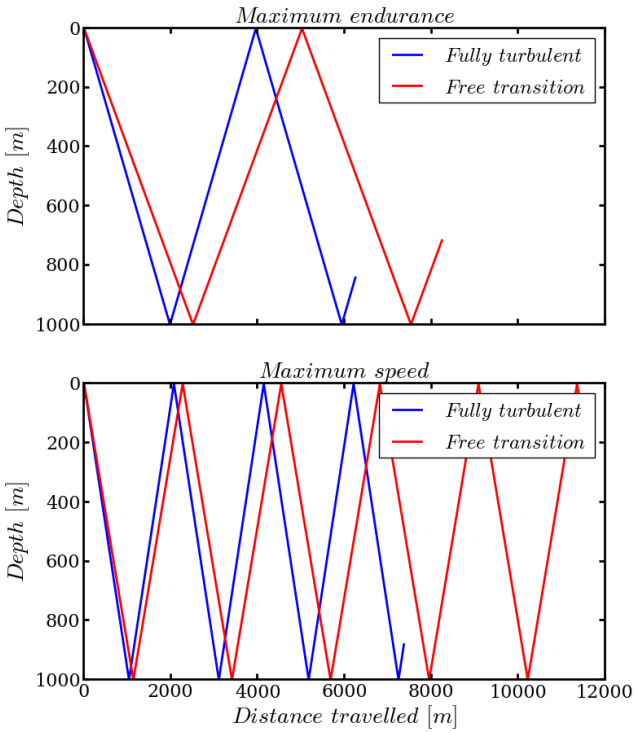

Fig. 17. Ascent and descent vehicle paths the selected glider is predicted to follow over a 5 hour period. Data obtained by assuming medium buoyancy engine actuation of 0.6% Δg, vertical amplitude of 1000 m, and computed for the fully-turbulent and free-to-transition flow simulation results.

15° trajectory which should yield maximum range. The data were computed by allowing the virtual vehicle to travel for a fixed period of 5 hours in each case. As expected from the velocity profiles, the free-transition data set, characterised by lower drag, yielded approximately 30% larger forward displacement of the vehicle. Also, one may clearly see in the data how keeping a shallow glide path angle reduces the forward speed and distance travelled in a fixed time, but reduces the number of pumping action at the top and bottom of each ascent and descent.

In order to obtain a more reliable metric of the range of the vehicle, it is necessary to account for the fact that it is limited by the capacity of its battery. This becomes drained by sustaining the hotel load necessary to operate the on-board electronics and sensors, as well as by operating the buoyancy engine pump. Total spent enrgy may therefore be expressed as a sum of the expenditures on the hotel load, E_{hotel}, and propulsion, $E_{propulsion}$,

$$E_{tot} = E_{hotel} + E_{propulsion}. \tag{5}$$

It is known from the literature that for a typical underwater glider between 60 and 80% of total power during a mission is spent on propulsion [6], [1], [7]. The present glider will carry a substantial amount of scientific payload beyond the standard CTD sensor, hence the lower bound of the aforementioned range was assumed, yielding the fraction of total power spent on propulsion of $f_P = 0.6$. It was also assumed that a typical motion profile of existing gliders is 1000 m deep. From the data presented by [4] for the Seaglider, a characteristic vertical speed for currently existing gliders was assumed to be 0.2 m·s^{-1}. This allows a simple relationship to be established between the hotel power, P_{hotel}, drawn and energy expense used to operate the pump during a single ascent or descent, $\Delta E_{prop} = f_P P_{hotel} \frac{1000}{0.2}$.

Thus, each of the terms in Eq. (5) could be computed for the present glider, given an assumed trajectory, like the ones presented in Figure 17, yielding

$$E_{tot} = \sum_{i=1}^{N_{tacks}} (P_{hotel}\Delta t_i + \Delta E_{prop,i}), \tag{6}$$

where Δt_i is the time taken by the glider to traverse a single ascent or descent and N_{tacks} is the total number of turns carrier out by the vehicle. Therefore, by assuming a fixed energy budget available to the glider, representative of a given battery size, total range of the vehicle could be computed for both maximum-speed and maximum-endurance locomotion modes of the glider. This was done by considering a range of amplitudes for the vertical motion, taking note of the fact that the presently designed glider will be capable of reaching depths up to 4500 m and could thus capitalise on the available height of the water column to achieve higher endurance. The predicted data are presented in Figure 18. It should be noted that the range has been shown as a relative quantity as the battery and power consumption data may not be disclosed.

As expected, the predicted range figures show the shallow glide path angle locomotion mode to yield higher endurance of the vehicle for motion amplitudes up to over 2000 m. However, as a larger part of the water column gets utilised for developing forward translation, the time between turns increases. This makes the relative proportion of the total energy spent coming from the hotel load rise and ultimately become the larger of the two power consumers. At this point it becomes more economical for the vehicle to accept travelling

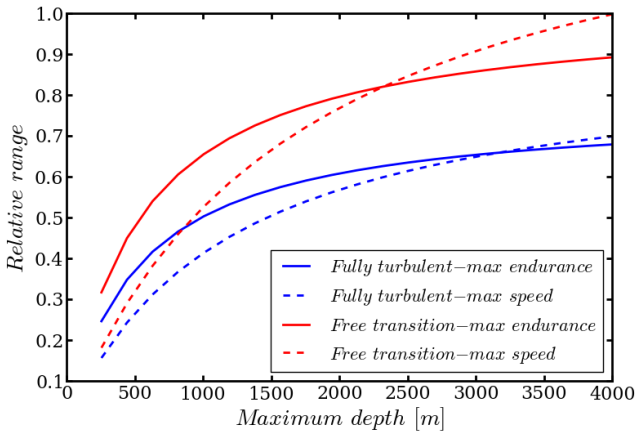

Fig. 18. Range predicted for the vehicle by assuming 60% of total energy is spent on propulsion during a typical 1000 m amplitude motion with vertical speed magnitude of 0.2 m·s^{-1}. Max endurance corresponds to shallow, 15° glide path angles and max speed scenario refers to the vehicle travelling at an inclination allowing the biggest possible forward velocity for a fixed buoyancy engine actuation. Estimates obtained using both sets of CFD results shown.

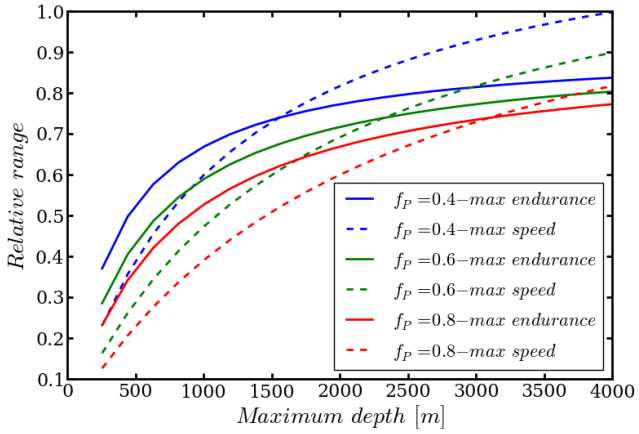

Fig. 19. Dependence of the predicted range on the assumed proportion of energy spent on propulsion, f_P, during a typical ascent or descent. Analysis uses the free-transition CFD data set and assumes a typical motion amplitude of 1000 m.

at steeper angles and performing more turns, which explains the higher endurance of the maximum-speed mode beyond this motion amplitude. An important point is that the present model assumes a fixed amount of energy spent per turn, thus ignoring the buoyancy engine actuation that will be needed to compensate for the larger changes in displaced volume and fluid density when performing very deep dives.

An important parameter in this part of the study is the assumed ratio of hotel and propulsive power consumptions, which will change the predicted range. In reality this would vary with the amount of sensors and on-board electronics being operated relative to the size of the fitted buoyancy engine. Increasing the ratio may also reflect how for deeper dives more energy will need to be spent on compensating for fluid density changes and hull compressibility. The effect of this assumption is studied in Figure 19 where three different values are considered. It is clear that reducing the proportion of energy spent on activating the buoyancy engine leads to increased range, irrespectively of whether the high-speed or high-endurance approach is followed. As might be expected, the more expensive the buoyancy engine actuation, the larger the motion amplitude needed to make the high-speed setting of the vehicle to yield longer range. This also indicates that as the additional pumping energy cost due to compressibility and density changes is factored in, the advantage of taking deeper dives will be reduced.

VII. Conclusions

It has been shown that computational fluid dynamics offer a useful tool in performing preliminary hydrodynamic analysis of underwater glider designs. Despite a relatively high cost per simulation, availability of high-power computing resources allowed the presented calculations to aid in developing a concept design for a new vehicle. The predictions also highlighted key areas that will require attention at future design stages.

The findings highlight the potential performance gains possible to achieve by encouraging natural laminar flow and by drag reduction in general. While it is possible to compensate for a drag increase with the use of larger, more powerful hydrofoils, only a fraction of their lift gets translated into useful forward thrust, particularly if shallower glide path angles are adopted. The majority of the lift is instead used to resist the upward motion and therefore such a solution requires the use of heavier buoyancy engines. In practice, achieving drag reduction through the use of natural laminar flow may prove difficult. Firstly, because it requires the overall shape of the design to be dictated by hydrodynamics, which often conflicts with the cylindrical profile of a typical pressure vessel, for instance. Furthermore, an underwater glider is first and foremost a sensor platform. However, many scientific payloads, such as conductivity, temperature and depth (CTD) sensors or turbulence probes need to be pointed into the flow through protrusions in the vehicle hull. These act locally to generate turbulence and make maintaining laminar flow challenging. Finally, in order to maintain favourable hydrodynamic characteristics in service, careful rules for assembly, disassembly, repair and maintenance would be required of the operators to ensure local imperfections stimulating early transition do not accumulate over time. It is therefore important to develop further understanding of how the practical design aspects may be dealt with in order to increase performance of next generation of this class of marine vehicles.

Exploring the expected flight trajectories of the proposed vehicle has indicated minimising the amount of energy spent on activating the buoyancy engine noticeably increases the vehicle endurance, irrespective of the trajectory it follows. Furthermore, it has been shown that due to its large depth rating, the present vehicle may potentially be able to move at relatively high glide path angles and corresponding high forward velocities, compared to gliders currently in common use, while still maintaining high endurance. Being able to do so would require the vehicle to be able to cope with changes in buoyancy due to compressibility and water density with minimum pumping effort, however. Taking advantage of the high pressure rating is also dependent on the available depth

of the water column and would come at a cost of not being able to sample data in the most interesting layer of the ocean within the first few hundreds of metres from the surface. It should, however, allow delivery of scientific payloads to remote locations in the deep ocean, performing local missions, and then returning to base faster.

ACKNOWLEDGMENTS

The presented work has been funded as a part of the BRIDGES Project (http://www.bridges-h2020.eu/). This Project has received funding from the European Unions Horizon 2020 research and innovation programme under grant agreement No 635359. The authors wish to acknowledge the use of the IRIDIS High Performance Computing Facility, and associated support services at the University of Southampton, in the completion of this work and the use of OpenFOAM (http://openfoam.org/) for all of the presented simulations.

All data supporting this study are openly available from the University of Southampton repository at http://doi.org/10.5258/SOTON/D0180.

REFERENCES

[1] D. L. Rudnick, R. E. Davis, C. C. Eriksen, D. M. Fratantoni, and M. J. Perry, "Underwater Gliders for Ocean Research," *Marine Technology Society Journal*, vol. 38, no. 2, pp. 73–84, 2004.

[2] S. Wood, *Autonomous Underwater Gliders*. Vienna, Austria: INTECH Open Access Publisher, 2009.

[3] J. Sherman, R. E. Davis, W. B. Owens, and J. Valdes, "The autonomous underwater glider," *Oceanic Engineering, IEEE Journal of*, vol. 26, no. 4, pp. 437–446, 2001.

[4] R. E. Davis, C. C. Eriksen, and C. P. Jones, "Autonomous Buoyancy-driven Underwater Gliders," *The technology and applications of autonomous underwater vehicles*, pp. 37–58, 2002.

[5] G. Griffiths, C. P. Jones, J. Ferguson, and N. Bose, "Undersea gliders," *Journal of Ocean Technology*, vol. 2, no. 2, pp. 64–75, 2007.

[6] J. G. Graver, *Underwater gliders - dynamics, control and design*. PhD thesis, Department of Mechanical and Aerospace Engineering, Princeton University, 2005.

[7] C. C. Eriksen, "Autonomous Underwater Gliders," in *Autonomous and Lagrangian Platforms and Sensors (ALPS) Workshop*, (31 March - 2 April, Sea Lodge, La Jolla, CA, USA), pp. 1–5, 2003.

[8] M. Rosenfeld, M. Wolfshtein, and M. Israeli, "A numerical study of the laminar incompressible flow over a 6:1 prolate spheroid at 10 degrees incidence," *Int. J. for Numerical Methods in Fluids*, vol. 15, no. December, pp. 147–173, 1992.

[9] C. C. Eriksen, T. J. Osse, R. D. Light, T. Wen, T. W. Lehman, P. L. Sabin, J. W. Ballard, and A. M. Chiodi, "Seaglider : A Long-Range Autonomous Underwater Vehicle for Oceanographic Research," *IEEE Journal of Oceanic Engineering*, vol. 26, no. 4, pp. 424–436, 2001.

[10] A. B. Phillips, S. R. Turnock, and M. Furlong, "The use of computational fluid dynamics to aid cost-effective hydrodynamic design of autonomous underwater vehicles," *Proc. IMechE Part M: J. Engineering for the Maritime Environment*, vol. 224, pp. 239–254, 2010.

[11] R. M. Hubbard, "Hydrodynamics technology for an advanced expendable mobile target (AEMT)," tech. rep., Rep. no. APL-UW 8013, Applied Physics Laboratory, University of Washington, Washington, DC, USA, 1980.

[12] A. Alvarez, A. Caffaz, A. Caiti, G. Casalino, L. Gualdesi, A. Turetta, and R. Viviani, "Folaga: A low-cost autonomous underwater vehicle combining glider Fo and AUV capabilities," *Ocean Engineering*, vol. 36, pp. 24–38, 2009.

[13] P. Jagadeesh, K. Murali, and V. G. Idichandy, "Experimental investigation of hydrodynamic force coefficients over AUV hull form," *Ocean Engineering*, vol. 36, pp. 113–118, 2009.

[14] S. A. Malik and P. Guang, "Transient Numerical Simulations for Hydrodynamic Derivatives Predictions of an Axisymmetric Submersible Vehicle," *Research Journal of Applied Sciences, Engineering and Technology*, vol. 5, no. 21, pp. 5003–5011, 2013.

[15] A. Phillips, M. Furlong, and S. R. Turnock, "The Use of Computational Fluid Dynamics to Assess the Hull Resistance of Concept Autonomous Underwater Vehicles," in *Oceans 2007-Europe*, 2007.

[16] J. V. N. de Sousa, A. R. L. de Macedo, W. F. de Amorim Junior, and d. L. A. G. B, "Numerical Analysis of Turbulent Fluid Flow and Drag Coefficient for Optimizing the AUV Hull Design," *Open Journal of Fluid Dynamics*, vol. 4, no. September, pp. 263–277, 2014.

[17] S. Tang, T. Ura, T. Nakatani, B. Thornton, and T. Jiang, "Estimation of the hydrodynamic coefficients of the complex-shaped autonomous underwater vehicle TUNA-SAND," *Journal of Marine Science and Technology*, vol. 14, no. 3, pp. 373–386, 2009.

[18] J. S. Parsons, R. E. Goodsont, and F. R. Goldschmiedt, "Shaping of Axisymmetric Bodies for Minimum Drag in Incompressible Flow," *Journal of Hydronautics*, vol. 8, no. 3, pp. 100–107, 1974.

[19] R. B. Langtry, *A correlation-based transition model using local variables for unstructured parallelized CFD codes*. PhD thesis, University of Stuttgart, 2006.

[20] J. Dantas and E. de Barros, "Numerical analysis of control surface effects on AUV manoeuvrability," *Applied Ocean Research*, vol. 42, pp. 168–181, 2013.

[21] B. Moat, D. Smeed, C. Marcinko, S. Popinet, and S. Turnock, "Flow distortion around underwater gliders and impacts on sensor measurements: a pilot study using large-eddy simulations (National Oceanography Centre Research and Consultancy Report, 58)," tech. rep., Research and Consultancy Report 58, National Oceanography Centre, Southampton, UK, 2016.

[22] D. K. Walters and D. Cokljat, "A Three-Equation Eddy-Viscosity Model for Reynolds-Averaged NavierStokes Simulations of Transitional Flow," *Journal of Fluids Engineering*, vol. 130, no. 12, p. 121401, 2008.

[23] The OpenFOAM Foundation, "OpenFOAM," 2014.

[24] F. Menter, "Two-equation eddy-viscosity turbulence models for engineering applications," *AIAA Journal*, vol. 32, no. 8, pp. 1598–1605, 1994.

[25] C. Badoe, B. Winden, A. Lidtke, A. Phillips, D. Hudson, and S. Turnock, "Comparison of various approaches to numerical simulation of ship resistance and propulsion," in *SIMMAN Workshop*, (December, FORCE Technology, Denmark), p. 7, 2014.

[26] A. Lidtke, A. Lakshmynarayanana, J. Camilleri, J. Banks, A. Phillips, S. Turnock, and C. Badoe, "RANS computations of flow around a bulk carrier with energy saving device," in *Tokyo 2015 Workshop on CFD in Ship Hydrodynamics*, (December 2-4, NMRI, Tokyo, Japan), p. 7, 2015.

[27] I. Pointwise, "Pointwise," 2016.

[28] Coupland, P. E. Roach, D. H. Brierley, and I. Ryhming, "ERCOFTAC T3 Case," 1990.

[29] S. S. Dodbele and C. P. van Dam, "Design of fuselage shapes for Natural Laminar Flow," tech. rep., Vigyan Research Associated Inc., NASA Contractor Report 3970, Hampton, VA, 1986.

[30] M. V. Ol, B. R. McCauliffe, E. S. Hanff, U. Scholz, and C. Kähler, "Comparison of Laminar Separation Bubble Measurements on a Low Reynolds Number Airfoil in Three Facilities," *35th AIAA Fluid Dynamics Conference and Exhibit*, pp. 1–11, 2005.

[31] M. S. Selig, J. J. Guglielmo, A. P. Broeren, and P. Giguere, *Summary of Low-speed airfoil data, volume 1*. Virginia Beach, Virginia: SoarTech Publications, 1995.

[32] A. K. Lidtke, S. R. Turnock, and J. Downes, "Assessment of Underwater Glider Performance Through Viscous Computational Fluid Dynamics," in *Autonomous Underwater Vehicles 2016 (AUV)*, (6-9 November, IIS, the University of Tokyo, Tokyo, Japan), 2016.

[33] D. F. Myring, "A theoretical study of the effects of body shape and Mach number on the drag of bodies of revolution in subcritical axisymmetric flow," tech. rep., Report no. 81005, Royal Aircraft Establishment, Farnborough, Hants, 1981.

[34] S. Lemaire, A. K. Lidtke, G. Vaz, and S. R. Turnock, "Modelling Natural Transition on Hydrofoils for Application in Underwater Gliders," in *19th Numerical Towing Tank Symposium (NuTTS)*, (3-4 October, St Pierre d'Oleron, France), p. 6, 2016.

[35] S. A. Jenkins, D. E. Humphreys, J. Sherman, J. Osse, C. Jones, N. Leonard, J. Graver, R. Bachmayer, T. Clem, P. Carroll, P. Davis, J. Berry, P. Worley, and J. Wasyl, "Underwater Glider System Study," tech. rep., Rep. no. 53, Scripps Institution of Oceanography, San Diego, CA, USA, 2003.